Wind Waves and Moveable-Bed Bottom Friction*

HENDRIK L. TOLMAN**

Marine Prediction Branch, Development Division, NOAA/NMC, Camp Springs, Maryland

(Manuscript received 12 February 1993, in final form 20 September 1993)

ABSTRACT

Effects of moveable-bed bottom friction for wave observations and wave modeling are investigated using a state-of-the-art bottom friction model. This model combines the hydrodynamic friction model of Madsen et al. with a moveable-bed roughness model based on Grant and Madsen. Analyzing the present model for idealized swell cases, it is shown that swell might result in wave-generated sand ripples. The large change of roughness corresponding to initial ripple formation results in a preferred wave height for swell, related to bathymetric scales as generally occur in shelf seas away from the coast. The corresponding wave-generated bottom roughness is not defined by the local wave conditions, but is related to the overall energy balance of the wave field. Sediment data thus is imperative for the interpretation of observed decay rates and friction factors for swell. For idealized depth-limited wind seas, near-bottom wave motion is expected to generate partially washed-out ripples and moderate sheet-flow roughness. A comparison with previous models explains the apparent success of several models that do not explicitly account for moveable-bed effects. Such models, however, are not expected to reproduce the above preferred wave-height concept.

1. Introduction

Wind waves in oceans are generally described using a spectral energy or action balance equation, accounting for linear wave propagation and source terms. The source terms describe wind input, wave–wave interactions, and wave breaking (whitecapping) (e.g., SWAMP Group 1985). The limited depths in shelf seas introduce modifications to the above source terms and introduce additional processes in the energy balance equation; propagation incorporates effects of shoaling and refraction and wave–bottom interactions provide additional mechanisms for wave energy dissipation (e.g., SWIM Group 1985). An early review of wave–bottom interactions is given by Shemdin et al. (1978), who consider percolation, bottom motion, bottom friction, and scattering of wave energy. For sandy bottoms, as found in many shelf seas, Shemdin et al. (1978) expect bottom friction to be dominant, in particular when the near-bottom wave motion is sufficiently strong to generate sediment transport and corresponding bed forms (ripple formation). Because the boundary-layer flow is (expected to be) rough turbulent for most interesting cases, bottom friction is a function of the equivalent bottom roughness k_N only. This roughness length can (theoretically) vary from sand grain roughness (order of 10^{-4} m) to ripple roughness (order of 10^{-2} to 10^{-1} m). Based on this range of roughnesses, Shemdin et al. (1978) concluded that decay rates due to bottom friction might vary by two orders of magnitude, which they found to be consistent with the wide range of observed decay rates for swell over sandy bottoms.

In the past decades, several bottom-friction models have been developed for irregular waves. A review is given by Weber (1991a,b). With a single exception (see below), all these models concentrate on the hydrodynamic aspects of bottom friction, assuming that the physical properties of the bottom, in particular k_N, are known. On the other hand, ripple formation due to waves (and currents) is extensively studied, mainly in the context of sediment transport. For monochromatic waves, a model for ripple formation and apparent roughnesses due to a thin layer of highly concentrated, saltating, and suspended sediment (i.e., sheet flow) has been developed by Grant and Madsen (1982). This model is more or less established in the sediment transport community. It has been applied in the wind wave model of Graber and Madsen (1988), in combination with a "representative monochromatic wave" to describe the spectrum (Madsen et al. 1988). Numerical experiments with a similar approach have been reported by Tolman (1989). However, several papers indicate that the Grant and Madsen model describes ripple formation for irregular waves inadequately. Recent studies on sheet flow also question the validity of the corresponding part of the Grant and Madsen model.

* OPC Contribution Number 82.

** UCAR Visiting Scientist.

Corresponding author address: Dr. Hendrik L. Tolman, NOAA/NMC21, Room 206, 5200 Auth Road, Camp Springs, MD 20746.

The present paper seeks to investigate moveable-bed roughnesses from a perspective of wind wave observations and (numerical) wind wave modeling (without resorting to full numerical models). In sections 2 and 3 hydrodynamic and roughness models are discussed to define a state-of-the-art model. The resulting model consists of the hydrodynamic model of Madsen et al. (1988) and a modified version of the Grant and Madsen (1982) roughness model. In section 4 the behavior of the present model is analyzed by assessing the occurrence of roughness regimes and by analyzing length scales of decay. For convenience of discussion, a distinction is made between swell and wind seas. Relevant decay scales for swell are found for both smooth beds (no sediment movement) and extremely rough beds (initial ripple formation). For wind seas relevant decay scales are expected to be accompanied by washed-out ripples and possibly by moderate sheet-flow roughness. Implications for wave observations and wave modeling are assessed in more detail in section 5. The discontinuous change of roughness related to initial ripple formation is shown to result in the occurrence of a preferred swell height, in particular for bathymetric scales as encountered in shelf seas away from the coast. In such conditions the actual roughness is determined by the overall energy balance (i.e., not by the local wave conditions only). Furthermore, it is shown that several previous models without explicit moveable-bed effects are expected to give generally good results, although neither of these models is expected to reproduce the above concept of a preferred wave height. The discussion in section 6 finally deals with implications of simplifications and uncertainties of the present model on the results, and with difficulties surrounding the implementation of a moveable-bed roughness model in a numerical wind wave model.

2. Hydrodynamic models

In the past decades, several (hydrodynamic) bottom-friction source terms for wind waves have been suggested, including an empirical model (Hasselmann et al. 1973), drag-law models (Hasselmann and Collins 1968; Collins 1972; Madsen et al. 1988), and eddy viscosity models (Weber 1991a,b). All these models share the following general form of the (two-dimensional) dissipation source term S (Weber 1991a,b)

$$S = -C\frac{k}{\sinh 2kd}F, \tag{1}$$

where k is the wavenumber of the spectral component, d is the mean water depth, F is the two-dimensional surface elevation spectrum [for instance, the vector wavenumber spectrum $F(\mathbf{k})$ or the frequency–direction spectrum $F(f, \theta)$], and C is a (model dependent) dissipation coefficient with the dimension of a velocity (henceforth denoted as the velocity scale). Note that the source term is actually related to the near-bottom velocity spectrum, which in the linear theory is defined as

$$\left(\frac{\sigma}{\sinh kd}\right)^2 F = 2g\frac{k}{\sinh 2kd}F,$$

where σ is the angular frequency of the spectral component [$\sigma^2 = gk\tanh(kd)$].

In the simplest model available, that is, the empirical JONSWAP model (Hasselmann et al. 1973), C is assumed to be a universal constant. As this formulation does not promote insight into the physics involved, and as more recent work indicates that C is not a universal constant (e.g., Bouws and Komen 1983) it will not be considered in this section.

For the drag-law models mentioned above, the velocity scale $C = f_w u_{b,r}$, where f_w is the friction factor[1] and where $u_{b,r}$ is a representative near-bottom velocity. The friction factor relates the bottom stress τ to the near-bottom velocity u_b; for example, $|\tau| = \frac{1}{2} f_w u_b^2$. A complicating factor in intercomparing drag-law models is that the representative velocity $u_{b,r}$ depends on the actual definition of the drag law, making friction factor formulations specific for the corresponding model. However, a generalized friction factor $f_{w,g}$ can be defined using a generalized near-bottom velocity $u_{b,g}$ independent of the drag law:

$$f_{w,g} = \frac{C}{u_{b,g}} = f_w\frac{u_{b,r}}{u_{b,g}}. \tag{2}$$

Note that such a generalized friction factor can be defined for any model, including eddy viscosity or empirical models. For most of the models mentioned above, $f_{w,g}$ is either a constant or a function of the nondimensional bottom roughness $k_N\sigma_{b,p}/u_{b,g}$ or $k_N/a_{b,g}$, where k_N is the (Nikuradse equivalent sand grain) roughness length, $\sigma_{b,p}$ is the peak frequency of the near-bottom spectrum, and $a_{b,r}$ is a representative near-bottom orbital excursion.

In Fig. 1, generalized friction factors $f_{w,g}$ are presented for several published bottom-friction source terms. The velocity $u_{b,g}$ is arbitrarily chosen to be the rms velocity u_{rms} and it is assumed that $u_{\text{rms}}/\sigma_{b,p} \approx a_{\text{rms}}$, where a_{rms} is the near-bottom rms orbital excursion. Note that the assumption of a rough turbulent boundary layer implies that the friction factor has a maximum for a relative roughness of approximately 1. For larger relative roughnesses, f_w is usually kept constant (e.g., Jonsson 1980).

Hasselmann and Collins (1968) (shaded area, denoted as HC) assume the friction factor to be a universal constant. Their velocity $u_{b,r}$ varies with the wave direction, having a maximum that (approximately) coincides with the mean wave direction. Collins (1972)

[1] Note that several papers use $c_w \equiv 2f_w$ (e.g., Hasselmann and Collins 1968).

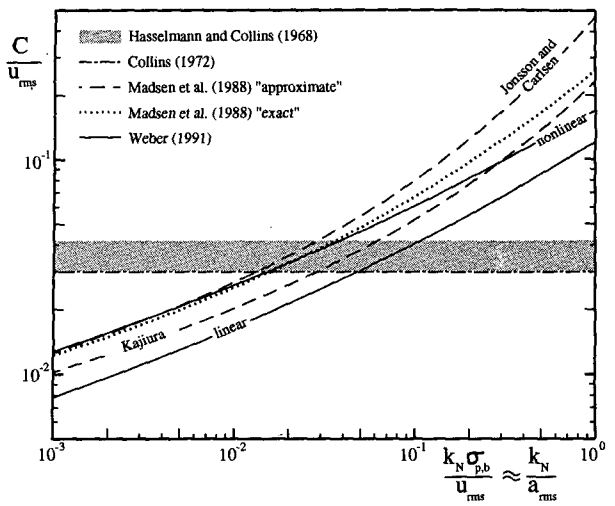

FIG. 1. General friction factor $C/u_{\rm rms}$ as a function of the relative roughness $k_N\sigma_{b,p}/u_{\rm rms}$. The "nonlinear" solution of Weber corresponds to the dominant stress direction; $C/u_{\rm rms}$ of Hasselmann and Collins varies with the spectral direction θ only.

(chain line, denoted as C) simplified this model by replacing $u_{b,r}$ with $u_{\rm rms}$.

The drag-law models of Madsen et al. (1988) incorporate friction factors that vary with the relative roughness. By design, this bottom-friction source term strongly resembles energy dissipation formulations for monochromatic waves. Without loss of generality, several semimonochromatic friction factor formulations can be used. Such formulations are obtained from the original formulations by replacing the monochromatic near-bottom velocity and excursion amplitudes with their rms values from the spectrum (note that the rms amplitude is by definition $\sqrt{2}$ times the overall rms parameter value). The dotted line in Fig. 1 represents the friction factor according to an "exact" formulation for the friction factor including 0th-order Kelvin functions [cf. Grant and Madsen (1979, 1982); our Eq. (4), denoted as MPG-E]. The dashed lines represent the well-known semiempirical formulation of Jonsson (1963, 1966) and Jonsson and Carlsen (1976) and the approximate rough-turbulent solution of Kajiura (1968) (equations not reproduced here). The latter formulations essentially are analytical approximations to the "exact" friction factor based on approximations to Kelvin functions and will be denoted as MPG-A.

Weber (1991a,b) presents fairly complicated "linear" and "nonlinear" eddy viscosity models, where the "(non)linear" identifies the dependence of the instantaneous stress on the random phase of the waves. Weber defines a simplified version of the linear model for application in wave models {lower solid line, denoted as WAL; Weber [1991b, Eqs. (3–15) and (B8)]; the simplifications imply that the spectral peak frequency is assumed to be representative for the entire spectrum, and that $u_{b,r}/u_{\rm rms}$ is approximately constant}. The nonlinear model incorporates a directional dependence similar to that of the HC model. Weber does not present a simplified nonlinear model. However, following the reasoning of Weber (1991a, p. 86) and using her Fig. 2, it follows that the linear model requires an approximately four times larger spectrum than the nonlinear approach to obtain identical values for C (main stress direction, assuming identical k_N and $\sigma_{b,p}$). Thus, $u_{\rm rms}$ of the linear model needs to be larger than $u_{\rm rms}$ of the nonlinear model by a factor of $\sqrt{4}$ to obtain identical values of C and $f_{w,g}$. For simplicity, assuming that $\sigma_{p,b}$ remains unchanged, an estimate of the nonlinear friction factors then follows directly from the approximate linear model by straightforward rescaling of the velocities (upper solid line, denoted as WAN).

The HC and C models start from a given friction factor, whereas all other models incorporate friction factors that are a function of the roughness k_N. As discussed by Shemdin et al. (1978), and as is commonly accepted for monochromatic waves, for example, Jonsson (1980), the latter approach is more realistic. Friction factors $f_{w,g}$ for the remaining models (solid, dashed, and dotted lines) differ by a (nearly constant) factor, which is smaller than 2 for $k_N\sigma_{p,b}/u_{\rm rms} < 0.1$. For $k_N\sigma_{p,b}/u_{\rm rms} > 0.1$, the MPG-A models (dashed lines) show the strongest dependence on the relative roughness. This behavior, however, is related to errors in the approximation to Kelvin functions on which MPG-A models are based (e.g., Weber 1991a; Christoffersen and Jonsson 1985). Because this roughness range is expected to be important for swell propagation (as will be shown below), such errors should be avoided. Thus, for theoretical reasons, the MPG-E, WAL, and WAN models are expected to represent the physics most accurately, while being simple enough to promote insight.

Only limited data is available on friction factors for spectra. Intercomparisons between model results and observations in nature as presented by Weber (1991b)

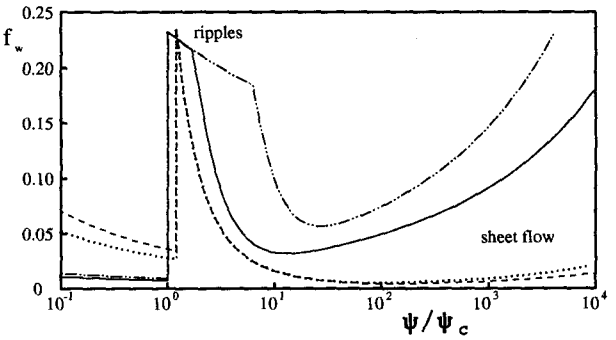

FIG. 2. Moveable-bed friction factors f_w as a function of the normalized Shields number ψ/ψ_c. The GM model as implemented by Graber and Madsen (1988) ($k_N = D$ for $\psi/\psi_c < 1$) for $D = 0.1$ mm (solid line) or $D = 0.4$ mm (chain line). Present model [Eqs. (9)–(14), $k_{N,0} = 0.01$] for $D = 0.1$ mm (dashed line) or $D = 0.4$ mm (dotted line). $T = 2\pi/\sigma_{b,p} = 10$ s, $\psi_c = 0.05$.

are interesting for intercomparing models, but are hardly suitable for model data comparison due to extremely coarse model resolution and the highly dissipative numerical propagation scheme. Some laboratory data for large relative roughnesses (Madsen and Rosengaus 1988; Madsen et al. 1990) shows friction factors $f_{w,g}$ of up to 0.3 for relative roughnesses close to 1, slightly favoring the MPG-E model (or some MPG-A models).[2] However, there is clearly insufficient data for a dependable model verification, in particular at smaller relative roughnesses. Thus, all models in Fig. 1 that are based on a roughness k_N show similar behavior and are effectively interchangeable in wind-wave modeling. Based on the limited data available, and for consistency with the ripple-roughness model presented in the following section, the MPG-E model will be used in the present analysis. In this model the source term S and the friction factor f_w are given as

$$S = -f_w u_r \frac{\sigma^2}{2g \sinh^2 kd} F, \tag{3}$$

$$f_w = \frac{0.08}{\mathrm{Ker}^2 2\sqrt{\zeta_0} + \mathrm{Kei}^2 2\sqrt{\zeta_0}}, \tag{4}$$

$$\zeta_0 = \frac{1}{21.2\kappa\sqrt{f_w}} \frac{k_N}{a_r}, \tag{5}$$

$$u_r = \left\{ \int \frac{2\sigma^2}{\sinh^2 kd} F \right\}^{1/2}, \tag{6}$$

$$a_r = \left\{ \int \frac{2}{\sinh^2 kd} F \right\}^{1/2}, \tag{7}$$

where Ker and Kei are Kelvin functions of the zeroth order and where κ is the von Kármán constant. The integration in Eqs. (6) and (7) is performed over the spectrum. Note that Eqs. (3)–(7) do not incorporate an implicit directional dependency, so that a one-dimensional spectrum is sufficient to evaluate the behavior of this model.

3. Bottom roughness

As discussed in the Introduction, ripple formation is expected to play an important role in wave energy dissipation due to bottom friction. Ripple formation has been studied for over a century. Reviews are given by Dingler and Inman (1976) and Grant and Madsen (1986). An extensive review of observed ripple types is given by Amos et al. (1988).

Ripple formation by waves is related to the ability of waves to move sediment, which in turn is governed by the Shields number ψ (e.g., Madsen and Grant 1976),

$$\psi = \frac{\tau_b'}{\rho(s-1)gD}, \tag{8}$$

where τ_b is the bottom friction, ρ is the density of water, s is the relative density of the sediment ρ_s/ρ (= 2.65 for quartz sands), and D is the representative grain diameter. The prime indicates values based on skin friction; that is, $k_N = D$. Sediment motion starts when the Shields number becomes larger than its critical value ψ_c, which is estimated as $\psi_c \approx 0.04 \sim 0.06$ for clean, well-sorted sands (e.g., Madsen and Grant 1976; Glenn and Grant 1987) and can become larger than 0.2 for bioturbated or multimodal sands (e.g., Drake and Cacchione 1986; Cacchione et al. 1987; Gross et al. 1992).

Grant and Madsen (1982, henceforth denoted as GM introduced a moveable-bed roughness model based on laboratory data for monochromatic waves without currents. In this model, the wave-induced roughness k_N becomes the sum of a ripple roughness k_r [GM Eqs. (8), (11), and (23) and Table 1] and a sheet-flow roughness k_s [GM Eq. (43)] (equations not reproduced here):

$$k_N = k_r + k_s. \tag{9}$$

To illustrate the effects of moveable-bed roughness on wave energy dissipation, friction factors for the GM model as implemented by Graber and Madsen (1988) are presented in Fig. 2. Note that Graber and Madsen (1988) use the hydrodynamic bottom-friction model of Madsen et al., so that their friction factors are consistent with the present model. Figure 2 shows small friction factors for wave conditions where no sediment movement occurs ($\psi < \psi_c$, roughness is assumed to be dominated by skin friction, $k_N = D$). At conditions of initial ripple formation ($\psi \approx \psi_c$), the relative roughness (discontinuously) becomes approximately 1, resulting in a friction factor $f_w \approx 0.23$. For increasing Shields numbers, the relative roughness decreases, so that f_w decreases until ripples are washed out completely. For $\psi/\psi_c = 10^1$ to 10^2, sheet flow starts to become important and f_w again increases with increasing Shields number.

Recent studies indicate shortcomings of the ripple- and sheet-flow roughness formulations of the GM model (as discussed below), in particular when applied to irregular waves. These studies also indicate possible improvements to the GM model for application to irregular waves.

The GM model relates ripple roughness to the ripple geometry, using empirical relations based on observations for monochromatic waves. These relations, however, are not expected to be valid for irregular waves for two reasons. First, many studies show that irregular waves result in shorter and less steep ripples than monochromatic waves (e.g., Dingler and Inman 1976; Nielsen 1981; Madsen et al. 1990; Ribberink and Al-Salem 1990, 1991). Second, Madsen et al. (1990) in-

[2] Note that for these observations $u_{b,r} = \sqrt{2}u_{\mathrm{rms}}$, so that $f_{w,g} = \sqrt{2}f_{w,\mathrm{observed}}$ [Eq. (2)].

dicate that irregular waves result in a hydrodynamically smoother bottom than monochromatic waves for identical ripple heights and steepnesses, which appears to be related to systematically different shapes of ripple crests. The latter difference between monochromatic and irregular waves makes it impossible to use the fairly abundant data on ripple geometry for irregular waves to construct an explicit ripple roughness model as in the GM model. Alternatively, the empirical relation of Madsen et al. (1990) will be used here:

$$\frac{k_r}{a_r} \approx 1.5\left(\frac{\psi}{\psi_c}\right)^{-2.5} \quad \text{for} \quad \frac{\psi}{\psi_c} \geq 1.2, \tag{10}$$

$$\psi = \frac{f'_w u_r^2}{2(s-1)gD}, \tag{11}$$

where f_w, u_r, and a_r are given by Eqs. (4), (6), and (7), respectively. The prime again indicates skin friction ($k_N = D$). Three remarks have to be made regarding Eq. (10). First, it was obtained by fitting observed friction factors based on Eq. (3) to the friction factor (4), which guarantees consistency with the present hydrodynamic model. Second, Madsen et al. found Eq. (10) to be fairly insensitive to the grain diameter D and to the spectral shape. Third, it should be noted that Eq. (10) is based on data with $\psi/\psi_c < 3$ only. As stressed by Madsen et al. (1990, p. 429), one should be careful to extrapolate to higher Shields numbers, although the similarity to the original GM model in the ripple break-off region somewhat supports extrapolation.

Presently, the most advanced model for sheet-flow roughness under oscillatory motion is given by Wilson (1989). Although sheet-flow conditions are not rough turbulent, an equivalent roughness (based on unidirectional flow data) can still be defined. Substituting the Shields number in Wilson's Eq. (8), the sheet-flow-induced roughness becomes

$$\frac{k_s}{a_r} = 5c_f \frac{u_r^2}{g(s-1)a_r}, \tag{12}$$

$$c_f = 0.114\left(\frac{a_r}{g(s-1)T^2}\right)^{0.4}, \tag{13}$$

where c_f is the friction factor for sheet flow and T is the wave period. Substituting (13) in (12) and using $T = 2\pi a_r/u_r$, the sheet-flow roughness becomes

$$\frac{k_s}{a_r} = 0.0655\left(\frac{u_r^2}{(s-1)ga_r}\right)^{1.4}. \tag{14}$$

Note that Eq. (14) is formally derived for monochromatic waves, where u_r and a_r are the near-bottom velocity and excursion amplitudes, respectively. Substituting Eqs. (6) and (7) for irregular waves constitutes an "equivalent wave" approach, consistent with the hydrodynamic model of Eqs. (3)–(7).

Equation (14) results in sheet-flow roughnesses smaller than those of the GM model by an order of magnitude. The apparent overestimation of the sheet-flow roughness by the GM model was previously observed and discussed by Wiberg and Rubin (1989), using field observations for unidirectional river flow. It is easily verified that Wilson's model shows excellent agreement with their data (Wiberg and Rubin, Table 1, $z_0 = k_N/30$). However, Wilson's model is based on unidirectional flow data only. Consequently, the choice of a sheet-flow roughness model presently remains somewhat arbitrary.

The moveable-bed roughness model defined by Eqs. (9)–(14) is valid only if wave motion is sufficiently strong to move sediment; that is, if $\psi/\psi_c \geq 1.2$. Otherwise the bottom roughness can be related to "relict ripples" of previous storm events (e.g., Drake and Cacchione 1989; Drake et al. 1992), current-induced roughness (e.g., Amos et al. 1988; Lyne et al. 1990; Drake et al. 1992), or bioturbation (e.g., Cacchione and Drake 1982; Grant et al. 1984; Grant and Madsen 1986; Cacchione et al. 1987; Amos et al. 1988). Ideally, this combined roughness should be modeled dynamically, which presently appears unfeasible. However, recognizing that the above processes will generally result in a bottom roughness $k_N \gg D$, a predefined "base" roughness $k_{N,0}$ will be adopted here for $\psi/\psi_c < 1.2$. The determination of $k_{N,0}$ is not straightforward. Roughnesses due to bioturbation, relict ripples, and current-induced ripples as presented in literature (e.g., Grant et al. 1984; Cacchione et al. 1987; Drake et al. 1992) are generally representative for mean currents. These roughnesses are not necessarily applicable to wave motion, in particular when the spacing of roughness elements is larger than the typical orbital excursion amplitude [e.g., Grant and Madsen (1979, p. 473); Grant and Madsen (1986, Table 1)]. In such cases, the wave roughness is expected to be closer to sand grain roughness and thus smaller than the corresponding current roughness. With estimated current roughnesses of typically 1–6 cm (e.g., Huntley and Hazen 1988; Cacchione et al. 1987), $k_{N,0}$ for $\psi/\psi_c < 1.2$ is expected to be of the order of 1 cm or smaller.

The behavior of the present roughness model as defined by Eqs. (9)–(14) is illustrated in Fig. 2, which furthermore shows the differences between the present model and the GM model as implemented by Graber and Madsen (1988). If no sediment movement occurs ($\psi < \psi_c$), the present model shows larger friction factors than the GM model as $k_{N,0} \gg D$. For initial ripple formation ($\psi \approx \psi_c$), both models show identically high friction factors. For larger Shields numbers, the present model shows smaller friction factors, due to smaller contributions of both ripples and sheet flow to the total roughness.

4. An analysis of the present model

In this section the behavior of the present model [Eqs. (3)–(11) and (14)] is analyzed with an emphasis

on effects of moveable beds. The expected occurrence of ripple and sheet flow conditions and spatial scales of energy decay are investigated. To obtain practical insight into the behavior of the present model, results are presented in terms of mean (surface) wave parameters such as the total energy $E = \int F$, the significant wave height $H_s = 4\sqrt{E}$, the peak wavenumber k_p ($=2\pi/L_p$), and frequency f_p ($=2\pi/T_p$) as a function of the depth d. For convenience of derivation and discussion, however, equations are generally expressed in terms of nondimensional quantities such as the relative depth $k_p d$. Furthermore a distinction will be made between swell and wind seas, where all swell energy is concentrated at f_p, and where wind seas are described using a TMA spectrum (Bouws et al. 1985). For wind seas the steepness is assumed to be constant (e.g., Bouws et al. 1985; Huang et al. 1983):

$$E \approx \frac{\epsilon}{4} k_p^{-2}, \tag{15}$$

where ϵ is the nondimensional energy level. Although this equation is derived for deep water, it is sufficiently accurate to obtain a general impression of depth-limited wind seas (see Bouws et al. 1985). From Eq. (15), the wave steepness in terms of H_s and L_p becomes

$$\frac{H_s}{L_p} \approx \frac{\sqrt{\epsilon}}{\pi}. \tag{16}$$

For $\epsilon = 0.015$ (fairly representative for young waves), this steepness becomes 0.039. For swell it is by definition much smaller.

a. *Wave-induced bottom roughness*

To investigate the occurrences of ripples and sheet flow, a_r, u_r, and the Shields number (11) are expressed in terms of the above mean wave parameters. Using the linear wave theory, a_r and u_r become

$$a_r = \frac{\alpha_a H_s}{2^{3/2}} \frac{1}{\sinh k_p d}, \tag{17}$$

$$u_r = \frac{\alpha_u H_s}{2} \left(\frac{g}{d} \frac{k_p d}{\sinh 2k_p d} \right)^{1/2}, \tag{18}$$

where α_a and α_u are shape factors depending on both $k_p d$ and the spectral shape. For swell both shape factors are by definition 1; for wind seas in shallow and intermediate depths they are typically somewhat smaller (see Fig. 3). Using (18), the Shields number (11) becomes

$$\psi = \frac{\alpha_u^2}{8(s-1)} \frac{H_s^2}{dD} f'_w \frac{k_p d}{\sinh 2k_p d}. \tag{19}$$

An expression for the critical wave height (H_c) required for initial ripple formation can be deduced from (19) by substituting $\psi = 1.2\psi_c$ and $H_s = H_c$:

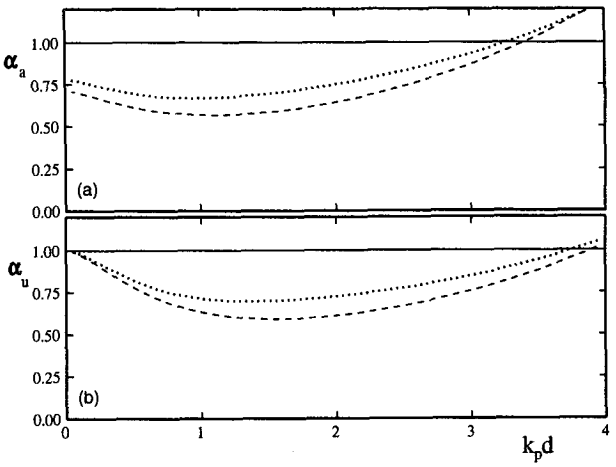

FIG. 3. Shape factors α_a and α_u [Eqs. (17) and (18)] as a function of the relative depth $k_p d$ and the spectral shape. Swell (solid line), TMA spectrum with $\gamma = 3.3$ (dotted line) and $\gamma = 1.0$ (dashed line), and $\sigma_a = \sigma_b = 0.08$.

$$\frac{H_c^2}{dD} = 8(s-1) \frac{1.2\psi_c}{\alpha_u^2 f'_w} \frac{\sinh 2k_p d}{k_p d}. \tag{20}$$

Considering that α_u is a weak function of $k_p d$ and the spectral shape and that f'_w corresponds to small relative roughnesses and hence is a weak function of D/a_r, Eq. (20) shows that H_c scales with $\psi_c^{1/2}$ and approximately scales with $D^{1/2}$. For small relative depths, $\sinh(2k_p d) \approx 2k_p d$, so that H_c becomes practically independent of the wave period and approximately scales with $d^{1/2}$. For large relative depths, however, the right side of Eq. (20) is dominated by the sinh factor, making H_c strongly dependent on the wave period and the (relative) depth.

In Fig. 4 critical wave heights H_c for swell are presented as a function of the depth d for several diameters D and periods T_p. Here H_c is fairly insensitive to the wave period T_p (Fig. 4a), as the low steepness of swell requires small relative depths to generate significant near-bottom wave motion but is sensitive to the grain diameter (Fig. 4b) and the depth. Note that the results of Fig. 4 (and Fig. 5) are representative for clean sand only ($\psi_c \approx 0.05$). Results for multimodal or bioturbated sands with larger values of ψ_c are obtained by rescaling H_c according to Eq. (20) ($H_c \div \psi_c^{1/2}$). The magnitude of H_c in Fig. 4 indicates that swell is expected to generate ripples in shallow water. The depth range for which ripples occur, however, depends strongly on the grain diameter D (Fig. 4b).

In Fig. 5a critical wave heights H_c for wind seas are presented for several diameters D [Eqs. (20) and (15) with $\epsilon = 0.015$]. For storm conditions ripples are expected to occur over a large range of depths, where the actual depth range again is strongly influenced by D. Extrapolation of this figure for the smaller diameters indicates that wave-induced ripples will occasionally

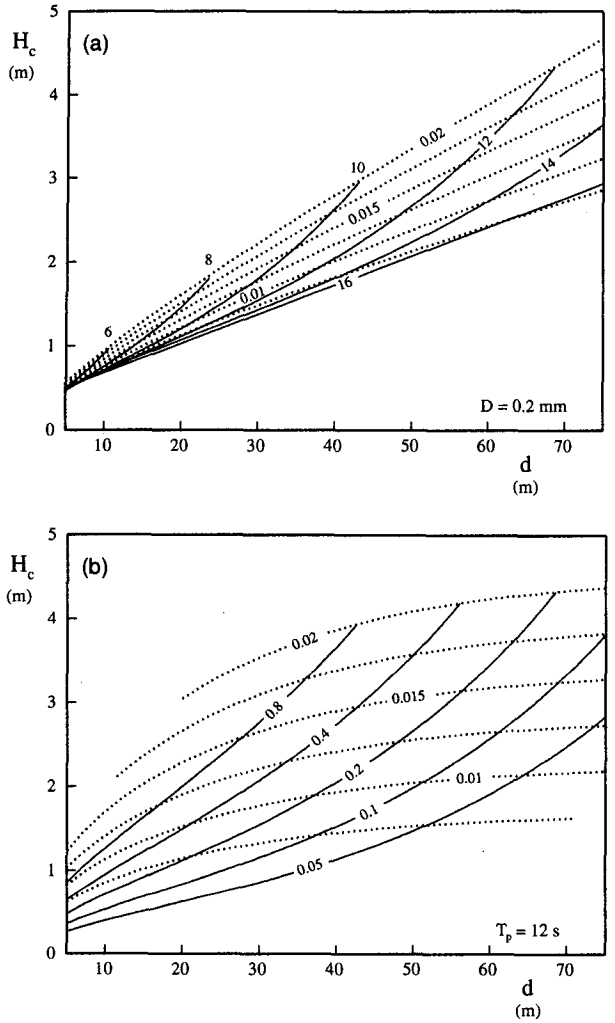

FIG. 4. Critical wave height for initial ripple formation (H_c) for swell. (a) For a given diameter $D = 0.2$ mm and various periods T_p (solid lines, periods in seconds). (b) For a period $T_p = 12$ s and various diameters (solid lines, diameters in millimeters). Dotted lines denote steepness H_s/L_p; $\psi_c = 0.05$, $s = 2.65$.

occur at depths as large as 100 m, as suggested by, for instance, Gross et al. (1992). In Fig. 5b the corresponding relative depths $k_p d$ are presented. The present model indicates that initial ripple formation due to wind seas is expected to occur for fairly large relative depths ($k_p d > 2$) in case of small grain diameters, but for more depth-limited conditions for the larger diameters considered.

Apart from the initial ripple formation, the occurrence of significant sheet flow roughness is of interest. A first estimate for the occurrence of sheet flow is found by defining a (fairly arbitrary) representative Shields number ψ_s for initial sheet flow. For swell a critical wave height for sheet flow $H_{c,s}$ is found by replacing ψ_c in Eq. (20) with ψ_s. Assuming (fairly arbitrarily) that $\psi_s/\psi_c \approx 25$ (see Fig. 2), $H_{c,s} \approx 5H_c$. Considering the wave heights in Fig. 4, this implies that realistic critical swell heights for sheet flow (i.e., of the order of 1 m) will occur only in extremely shallow water (depth order of several meters). Consequently, swell is expected to generate sheet flow conditions in the surf zone only. For wind waves, a direct rescaling of H_c is not representative, because H_s and T_p are related. Instead $H_{c,s}$ has to be calculated similar to H_c assuming a value for ψ_s/ψ_c. In Fig. 5 $H_{c,s}$ is presented for $D = 0.2$ mm and $\psi_s/\psi_c = 25$. This figure shows large but not unrealistic wave heights $H_{c,s}$, in particular for relatively small water depths. The corresponding Shields number, however, implies that ripples are expected to be mostly washed out but that sheet flow roughnesses are still moderate (Fig. 2). Even without further analysis, it

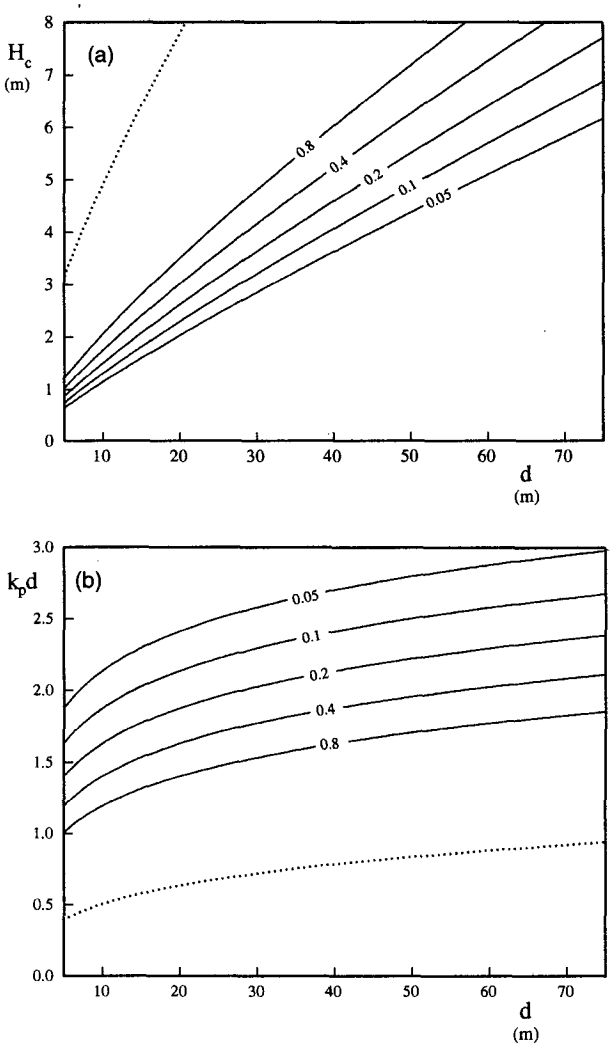

FIG. 5. Critical wave height for initial ripple formation H_c for wind seas [panel (a)] and the corresponding relative depth $k_p d$ [panel (b)] for several grain diameters (in millimeters). Here, $\epsilon = 0.015$, $\sigma_a = \sigma_b = 0.08$, $\gamma = 3.3$, $\psi_c = 0.05$, $s = 2.65$. The dotted line corresponds to the critical wave height for sheet flow ($H_{c,s}$) for $D = 0.2$ mm and $\psi_s/\psi_c = 25$.

appears unrealistic to expect wind waves to generate significant sheet-flow roughness, except for conditions with shallow water and rapidly changing depths (e.g., on a beach).

b. Spatial scales of wave energy decay

The importance of bottom friction for wind waves in the context of wave generation and dissipation can be assessed by considering spatial scales of wave energy decay. First, the total wave energy dissipation will be considered. The temporal scale of decay t_t for the total wave energy $E = \int F$ is defined as $t_t \equiv -E/S_t$, where $S_t = \int S$ (the suffix t is used for later comparison with scales within the spectrum). Using (3), (6), and (18), t_t can be expressed in terms of mean wave parameters as

$$t_t \equiv \frac{E}{-S_t} = \frac{2}{\alpha_u^3 g^{1/2}} \frac{d^{3/2}}{f_w H_s} \left(\frac{\sinh 2k_p d}{k_p d} \right)^{3/2}. \quad (21)$$

Note that the effect of wave-generated bottom roughness is absorbed in f_w. A spatial scale of decay x_t then is defined as $x_t = t_t c_{g,p}$, where $c_{g,p}$ is the group velocity for f_p. After some straightforward manipulations, x_t becomes ($n \equiv kc_g/\sigma$)

$$x_t = \frac{2\sqrt{2}}{\alpha_u^3} \frac{d^2}{f_w H_s} G(k_p d), \quad G(kd) = \frac{\sinh kd}{kd} \frac{2n}{2n-1}. \quad (22)$$

In Fig. 6 decay scales x_t as a function of depth d are presented for a typical swell with $H_s = 1$ m and $T_p = 12$ s for clean sand with $D = 0.2$ mm. The sensitivity of x_t to the latter three parameters is also shown. As follows from the results of the previous section, initial ripple formation occurs in the depth range considered. Initial ripple formation is identified in Fig. 6 by the discontinuous change of x_t by up to an order of magnitude. The depth of initial ripple formation is very sensitive to the wave height, but virtually independent of the wave period, as could have been inferred from (the discussion of) Fig. 4. Similarly, the decay scales depend mostly on the wave height and the bottom material. If no ripples occur, x_t is typically O(100 km); x_t related to ripple formation of O(10 km) or even smaller. Both decay scales are generally significant for swell propagation in shelf seas.

In Fig. 7 decay scales x_t as a function of depth d are presented for a range of wind sea wave heights and a grain diameter $D = 0.1$ mm (panel a) or $D = 0.4$ mm (panel b). If ripples occur, the spatial scales x_t for all wave heights are concentrated in a fairly narrow band, in particular for $D = 0.4$ mm. The spatial scale of decay is typically of O(10^1–10^2 km) and increases sharply with increasing depth. A situation without ripples occurs only for fairly low wave heights and large water depths. The corresponding decay length scales are O(10^3 km) or larger. The latter decay scales are generally irrelevant compared to bathymetric scales and scales of wave generation. Consequently, relevant bottom friction for wind waves over moveable beds corresponds to a washed-out ripple regime with moderate sheet-flow contributions.

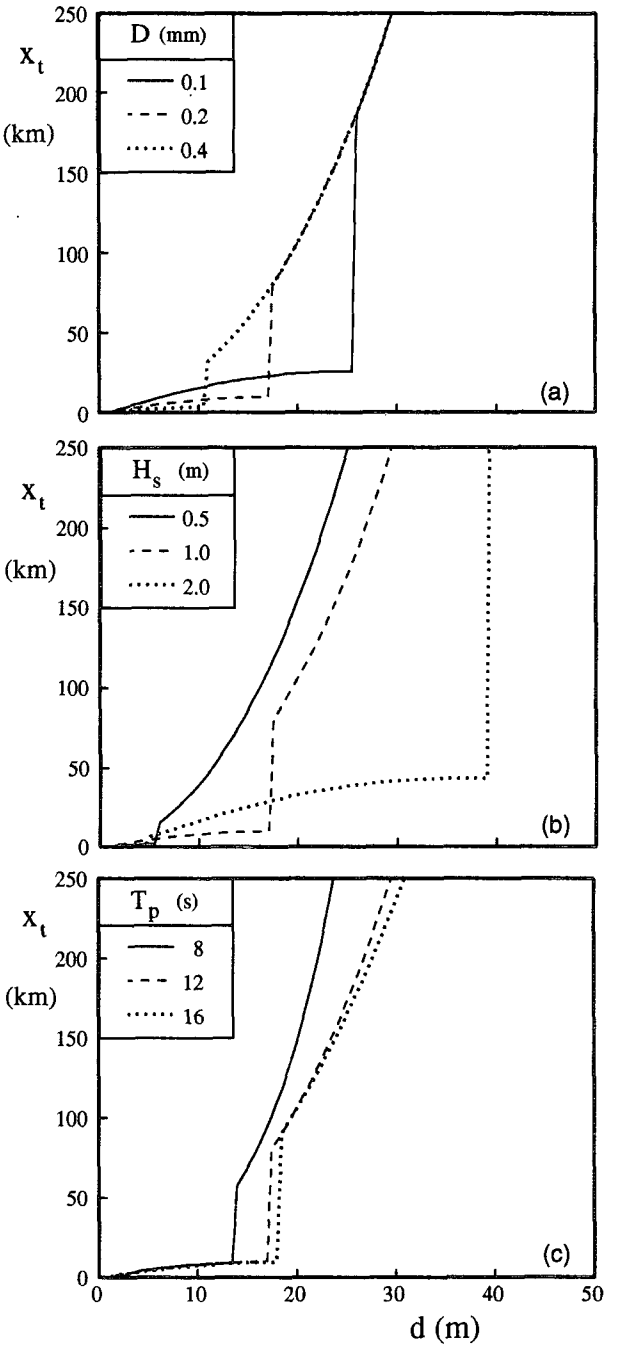

FIG. 6. Decay length scales x_t for swell on sandy bottoms with $\psi_c = 0.05$ and $k_{N,0} = 0.01$ m. Unless specified differently, $D = 0.2$ mm, $H_s = 1$ m, and $T_p = 12$ s.

Finally, the variation of effects of bottom friction within spectra is analyzed. For every spectral frequency

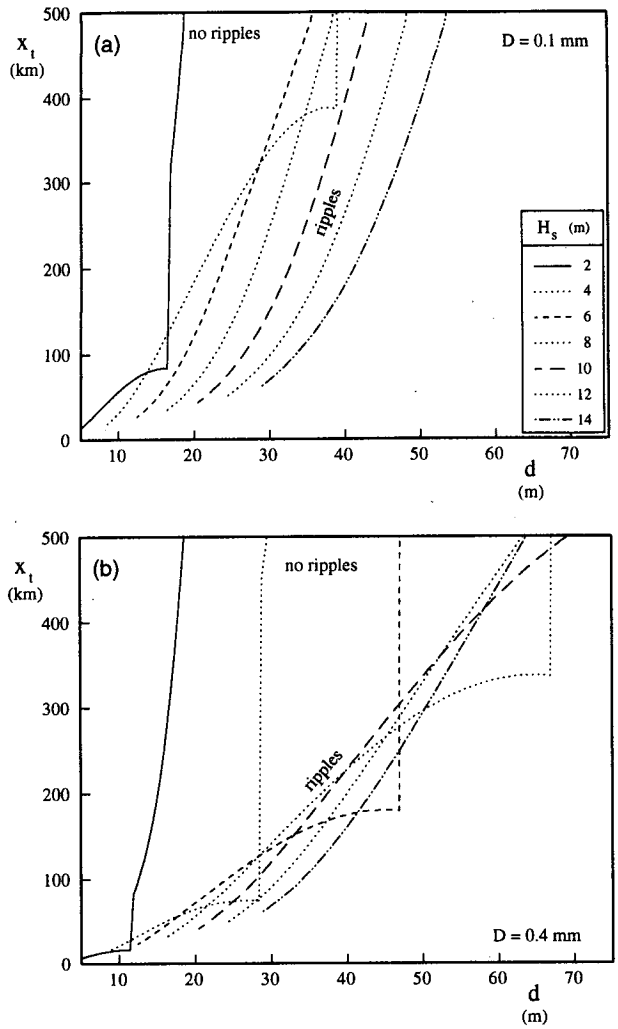

FIG. 7. Decay length scales x_t for wind seas on sandy bottoms for grain diameters $D = 0.1$ mm (panel a) or $D = 0.4$ mm (panel b): $k_{N,0} = 0.01$ m, other parameters as in Fig. 5. Results for $k_p d > 0.5$ only.

f a separate scale x_f can be defined. Using (3), (18), and (22), the intraspectral scale of decay x_f becomes

$$\frac{x_f}{x_t} = \alpha_u^2 \frac{H(kd)}{H(k_p d)}, \quad H(kd) = \frac{2n}{2n-1}\left(\frac{\tanh kd}{kd}\right)^{1/2}. \tag{23}$$

The normalized intraspectral scale of decay x_f/x_t is presented in Fig. 8. Two features of Fig. 8 are striking. First, decay length scales always decrease with decreasing frequencies. This implies that spectra moving from deep to shallow water will loose low frequency energy more rapidly that high frequency energy. Hence, effects of bottom friction will generally result in single-peaked wind sea spectra. Second, the intraspectral behavior of bottom friction varies significantly with the relative water depth $k_p d$. For larger depths (e.g., $k_p d \approx 2.5$), bottom friction acts as a filter function, removing low frequency energy much faster than high frequency energy. For smaller depths (e.g., $k_p d \approx 1$), however, decay length scales remain approximately constant for a large range of frequencies, influencing the entire spectrum in a similar fashion.

5. Implications for observations and modeling

Using the results of the previous section, implications of moveable-bed roughness for wind wave observations and wind wave modeling can be assessed.

Observations generally consider decay rates and friction factors for typical swell cases (e.g., Shemdin et al. 1978) or wave heights for typical depth-limited wind seas (e.g., Bouws and Komen 1983; Bouws et al. 1985). In both cases moveable-bed roughness might account for scatter in data, in particular where bottom friction is sensitive to sediment or wave parameters. Thus, the largest impact of moveable-bed effects is expected for conditions of initial ripple formation, which generally are relevant for swell observations only (section 4). In such conditions, the discontinuous model behavior complicates the interpretation of the results. This discontinuous behavior will be discussed in more detail in section 5a. For wind seas with relevant effects of bottom friction, the bottom roughness is generally expected to be well within the ripple regime (section 4). In such conditions the relative bottom roughness is generally small, making the bottom roughness (and hence the friction factor) fairly insensitive to sediment and wave parameters. Consequently, the variability in observations of depth-limited wave heights for wind seas is not expected to be dominated by moveable-bed effects. However, sediment conditions might explain differences between observations at different locations.

For modeling of wind waves the largest effects of moveable beds on bottom friction are obviously also

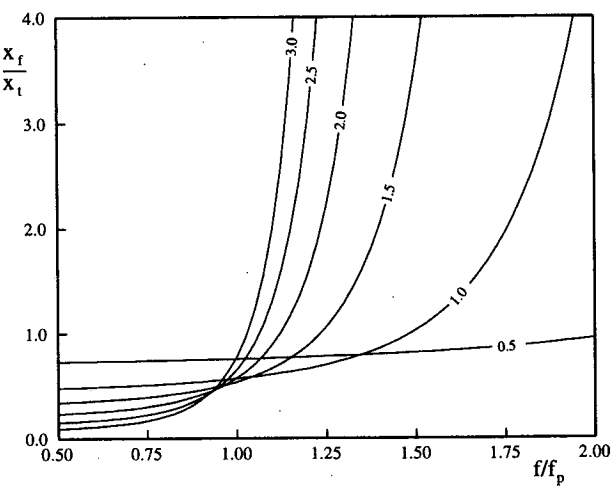

FIG. 8. Normalized intraspectral decay length scale x_f/x_t, as a function of the normalized frequency f/f_p.

expected for swell propagation in conditions of initial ripple formation. In a more general sense, however, it is interesting to compare previous models for bottom friction with the present model, to analyze differences, and explain the apparent success of previous models, which do not consider a specific bottom roughness measure at all. Therefore, a model intercomparison is presented in section 5b. Note that a distinction between swell and wind seas becomes less relevant for wave modeling in general; in many cases such a distinction cannot be made. The distinction is nevertheless illustrative, and will therefore be utilized further.

a. *Swell propagation and initial ripple formation*

The discontinuous change of the friction factor for $\psi/\psi_c = 1.2$ complicates both the interpretation of effects of moveable-bed roughness, and its modeling. The roughness and friction factor can assume any value within this discontinuous change, depending on the overall energy balance. This is explained as follows. Ripple generation is a dynamic process, where ripples build up, only when sediment movement occurs ($\psi/\psi_c > 1.2$). However, ripple buildup will increase energy dissipation and hence decrease the wave energy and ψ/ψ_c. If $\psi/\psi_c = 1.2$ is reached, ripple development will stop, regardless of the development state of the ripples. Hence, the actual roughness (and f_w) will depend on the overall energy balance of the wave field. This mechanism is expected to occur, if the bathymetric scales are of the same order of magnitude or larger than the decay scale x_t corresponding to fully developed initial ripples [typically O(10 km), Fig. 6], as is the case in many shelf seas away from the coast.

To illustrate the potential dependence of the roughness on the energy balance, a simple one-dimensional moveable-bed swell propagation model has been constructed (Appendix). In Fig. 9 results are presented for several swell systems with a period $T_p = 12$ s traveling over a bottom with a constant slope into shallow water (d ranges from 50 to 20 m over a distance of 100 km, $D = 0.2$ mm, $\psi_c = 0.05$). For the smaller water depths, several swell systems show a constant normalized Shields number $\psi/\psi_c = 1.2$, indicating conditions of initial ripple formation. The corresponding friction factors have values between those related to "smooth" beds ($f_w \approx 0.05$) and those related to fully developed ripples ($f_w \approx 0.23$), indicating that the friction factor is governed by the energy balance. The corresponding wave height can be calculated directly from $\psi/\psi_c = 1.2$, and thus equals the critical wave height H_c given by Eq. (20). In Fig. 9 the occurrence of a preferred wave height (H_c) in shallow water is obvious. This preferred wave height can, nevertheless, be exceeded if the decay scale becomes larger than the bathymetric scales. The latter occurs if bathymetric scales are reduced (i.e., for steeper slopes), or for higher wave heights (Fig. 6b). Furthermore, the preferred wave height is more easily

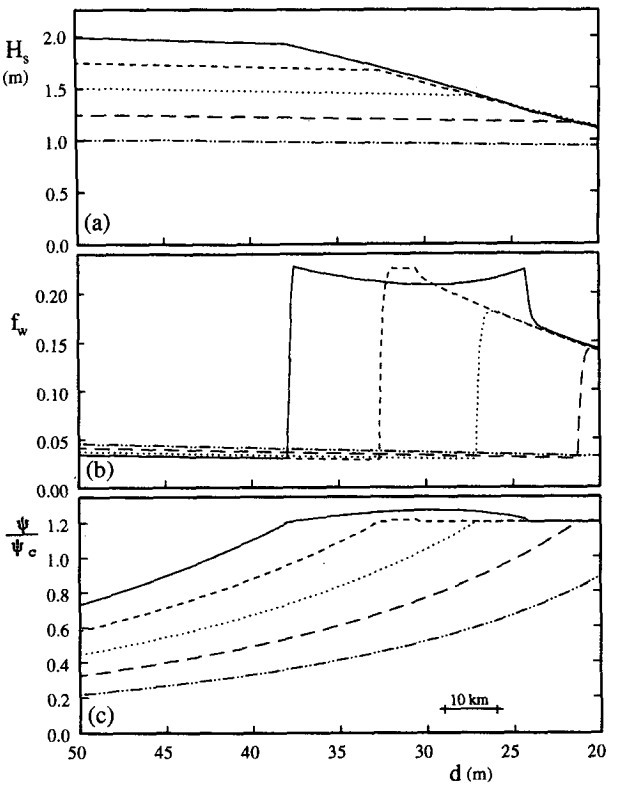

FIG. 9. Wave height H_s, friction factor f_w, and normalized Shields number ψ/ψ_c as a function of the depth d according to the swell propagation model of the Appendix for a bottom with constant slope and a depth ranging from 50 to 20 m over a distance of 100 km. $T_p = 12$ s, $D = 0.2$ mm, $\psi_c = 0.05$, and $k_{N,0} = 0.01$ m.

exceeded for smaller grain diameters because decay scales for fully developed ripples increase with decreasing grain diameter (Fig. 6a).

Considering the above, the friction factor related to the preferred wave height is not a locally defined measure for the bottom roughness but explicitly depends on the bathymetry (and hence on the wave propagation direction). Friction factors for swell are therefore not only potentially sensitive to sediment conditions, but sediment data is imperative for the interpretation of observations (or model results). The mechanism resulting in the preferred wave height also has an interesting implication for sediment transport and bottom roughness, as the preferred wave height can be accompanied by large roughnesses, but is by definition related to small sediment transports. In previous papers, however, large roughnesses are usually implied from large sediment concentrations (e.g., Cacchione et al. 1987; Gross et al. 1992).

b. *Behavior of previous bottom friction models*

In roughness regimes not related to initial ripple formation, effects of moveable-bed roughness on bottom

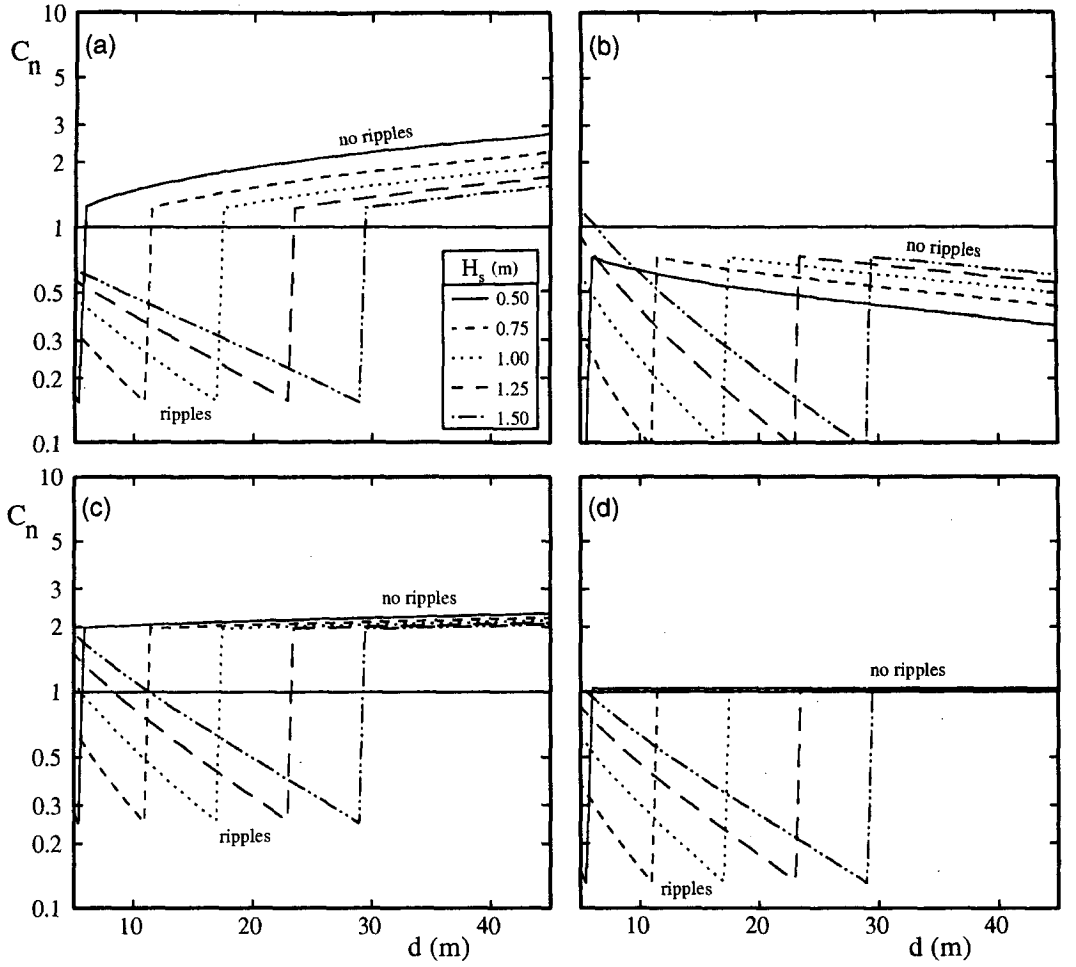

FIG. 10. Normalized velocity scales C_n ($= C_{old}/C_{new}$) for swell. (a) JONSWAP ($\Gamma = 0.038$ m^2 s^{-3}), (b) Collins (1972), (c) Madsen et al. (1988) ($k_N = 0.04$ m), and (d) the Weber (1991b) simplified linear eddy viscosity model ($k_N = 0.04$ m). $D = 0.2$ mm, $k_{N,0} = 0.01$ m, $\psi_c = 0.05$, $T_p = 12$ s, wave heights as given.

friction might be moderate. It is therefore interesting to examine, if previous models that do not explicitly account for the (moveable bed) bottom roughness are expected to give reasonable results. Equation (1) indicates that the ratio of source terms equals the normalized velocity scale C_n, that is, C of previous models normalized with C of the present model.

Four previous models will be compared to the present model. Fairly arbitrarily, the sediment parameters of the present model are set to $D = 0.2$ mm, $\psi_c = 0.05$, and $k_{N,0} = 0.01$ m. Note that the fairly arbitrary choice of the sediment parameters makes a strict model intercomparison difficult. Qualitative differences and trends, however, can be identified. The first model considered is the empirical JONSWAP model (Hasselmann et al. 1973), with the constant $\Gamma = \frac{1}{2} gC$ defined separately for swell ($\Gamma = 0.038$ m^2 s^{-3}, Hasselmann et al. 1973) and wind seas ($\Gamma = 0.067$ m^2 s^{-3}, Bouws and Komen 1983). The second model is the Collins (1972) approximation to the Hasselmann and Collins (1968) model ($C = 0.03 u_{rms}$, denoted as HCC). The third model is the Madsen et al. model [Eqs. (3)–(7) with a predefined roughness k_N, denoted as MPG]. In cases without ripples, this model is identical to the present model, if $k_N = k_{N,0}$. To assess the impact of the choice of roughness length, $k_N = 0.04$ m will be used here [as suggested by Weber (1991b) to be representative for the southern North Sea]. The final model is Weber's approximate linear eddy viscosity model [denoted as WAL, Weber (1991b), Eq. (3-15) and (B8)], also with $k_N = 0.04$ m.

In Fig. 10 normalized velocity scales C_n for the above four models are presented as a function of depth for swell with several wave heights and with $T_p = 12$ s. If no ripples occur, all four models show C_n fairly close to unity. The JONSWAP model (panel a) shows larger dissipation than the present model by up to a factor of 2 ($1 < C_n < 2$). The HCC model (panel b) shows smaller dissipation by up to a factor of 2.5 ($0.4 < C_n < 1$). The MPG model shows twice as much dissipation

as the present model ($C_n \approx 2$), due to the larger roughness ($k_N = 4k_{N,0}$). The WAL model is practically identical to the present model; effects of the larger roughness length ($k_N = 4k_{N,0}$) are balanced by the different friction factor (see Fig. 1). If ripples do occur, the previous models all underestimate dissipation by up to an order of magnitude ($C_n \ll 1$).

In Fig. 11 normalized velocity scales for wind seas are presented. As discussed above, bottom friction for wind seas is relevant only well within the ripple regime. The discussion of Fig. 11 therefore focuses on such conditions only. The JONSWAP model (panel a) shows good agreement with the present model ($C_n \approx 1$) well inside the ripple regime. This good agreement is explained from the interrelated behavior of u_r and f_w; an increase of u_r is usually accompanied by an increase in a_r and ψ [Eq. (11)] and hence a decrease of the ripple roughness [Eq. (10)] and the friction factor (Fig. 1 and Fig. 2). As variations in u_r and f_w largely cancel out, $C = f_w u_r$ is nearly constant, as assumed in the JONSWAP model. The HCC model (panel b) shows a systematical variation of C_n with depth (ripple regime), which is explained by the fact that C varies with u_r, but that such variations are by definition not balanced by variations in f_w. The MPG and WAL models (panels c and d) show behavior similar to that of the present model (C_n nearly constant well within the ripple regime), as variations of f_w are dominated by variations of a_r. As in the swell case without ripples, the MPG model shows larger dissipation than the present model ($C_n \approx 2$), whereas the WAL model is somewhat closer to the present model ($C_n \approx 1.3$).

Considering the above, $C = f_w u_r$ is fairly constant for many common roughness regimes. Furthermore, variations of the friction factor are mostly dominated by hydrodynamic effects rather than moveable-bed effects. This explains the apparent success of the JONSWAP model (Hasselmann et al. 1973), and makes use of a single predefined roughness [i.e., the models of Madsen et al. (1988) and Weber (1991a,b)] poten-

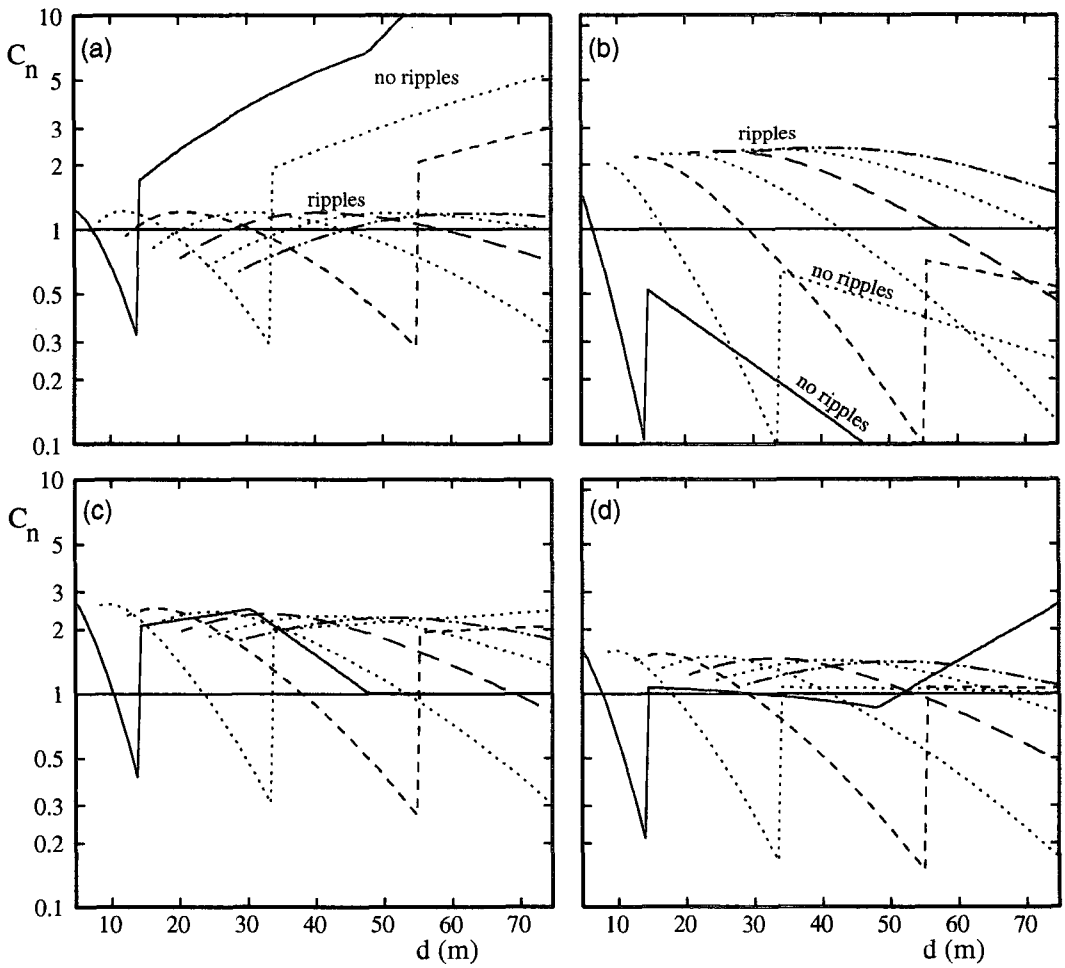

FIG. 11. As in Fig. 10 but for wind seas. Spectral parameters as in Fig. 5, legend as in Fig. 7, JONSWAP model with $\Gamma = 0.067$ m^2 s^{-3}.

tially successful. The above three models are therefore expected to be generally suitable for application in numerical wave models, after proper tuning of C or k_N. None of the above models, however, is expected to reproduce the above preferred wave height concept. The models of Hasselmann and Collins (1968) and Collins (1972) (constant friction factor), however, show systematically different behavior and are therefore not recommended for use in wave models. Note that the latter conclusion is mainly based on hydrodynamic considerations.

Two final remarks have to be made on the three preferred models. The JONSWAP model cannot be tuned universally (e.g., Bouws and Komen 1983), and should therefore be used for case studies only. The other two models are expected to show consistent behavior for swell and wind seas (Fig. 10 and Fig. 11, panels c and d), and are therefore suitable for general forecast and hindcast models. Optimally tuned roughness lengths k_N are furthermore related to the actual hydrodynamic model used, and therefore have a somewhat limited physical meaning.

6. Discussion

The present paper investigates the (potential) effects of moveable-bed roughnesses for observations and modeling of wind waves. The analysis is centered on the behavior of a poorly verified roughness model. Because the present conclusions stand or fall with the validity of this model, the sensitivity of the results to possible errors in the roughness model needs to be discussed. Three roughness regimes (i.e., ranges of Shields numbers) will be considered.

The large (jump in) roughness corresponding to initial ripple formation ($\psi/\psi_c \approx 1$) represents the best documented part of the model. Virtually all observations of ripple geometries at near-critical Shields numbers show the existence of extremely steep ripples (Dingler and Inman 1976; Nielsen 1981; Madsen et al. 1990; Ribberink and Al-Salem 1990, 1991). The expected friction factor is close to the maximum friction factor for rough-turbulent boundary layers (typically 0.2–0.3), as is verified by Madsen and Rosengaus (1988) and Madsen et al. (1990). Furthermore, the existence of a critical Shields number has been verified in nature (e.g., Drake and Cacchione 1986). Hence, all aspects of moveable-bed roughness leading to the concept of preferred swell heights are well documented with observations. Note that the prediction of this height is not trivial, due to difficulties in estimating D and ψ_c, in particular for multimodal and bioturbated sands.

For somewhat higher Shields numbers ($3 < \psi/\psi_c < 10$), only ripple-geometry observations are available (e.g., Nielsen 1981). As is shown by Madsen et al. (1990), such observations cannot easily be transformed to roughness observations. The observations, however, are clearly incompatible with the large roughnesses of the GM models so that errors in the present model are expected to be significantly smaller than the differences between the present and GM models in Fig. 2. This range of Shields numbers was found to be important mainly for higher swells. Although different roughnesses might influence the range of wave conditions for which a preferred wave height occurs, it is not expected to influence its concept.

Similarly, no roughness observations are available for even higher Shields numbers [$O(10^1$ to $10^2)$]. This range is particularly interesting for wind seas, where moveable-bed effects are not expected to have a large influence on the behavior of bottom friction, as follows from the model intercomparison in section 5b. This conclusion is related to the general model behavior, consisting of a fairly smooth, continuous variation of the roughness as a function of the normalized Shields number, where hydrodynamic variations of the friction factor for a constant roughness result in fairly realistic model behavior. As long as new observations do not identify new mechanisms of wave-generated roughness, the general behavior of wave-induced roughness is not expected to be systematically different from that of the present model. Consequently, the present conclusions for wind seas are not expected to be sensitive to errors in the roughness model.

It is thus not expected that the general conclusions of this study are sensitive to uncertainties in the (roughness) model. It is obvious though, that more observations are required to verify and refine the present model, if it is to be used in the analysis of observations or in numerical wave modeling.

A second potential shortcoming of the model is that effects of currents are neglected, although wind waves in shelf seas generally exist in an environment with significant tides and wind-driven currents. From a hydrodynamic point of view (i.e., for a given roughness k_N), effects of currents on the wave friction factor can generally be neglected, as predicted by models (Grant and Madsen 1979; Christoffersen and Jonsson 1985) and verified with observations (Nielsen 1992, section 1.5.6; Tolman 1992, 1993; Simons et al. 1992). However, wave–current interactions through bed forms are likely to occur. Current-induced ripples form (part of) the base roughness of the present model, which is expected to be important for swell propagation only. Furthermore, currents might influence initial ripple formation by waves. Ripple observations of Amos et al. (1988), however, suggest that such effects are small. Finally, current-induced bed forms are expected to be unimportant for depth-limited wind waves, as intense wave motion is expected to wash out all bed forms.

Implementation of moveable-bed roughnesses in numerical wave models might be desirable, in particular when swell propagation away from the coast is considered. Two complications hamper implementation of a moveable-bed friction model in a numerical

wave model, (i) the sediment data required and (ii) the discontinuous model behavior at initial ripple formation with its corresponding small decay scales.

Sediment data is generally sparse, in particular, where the critical Shields number is considered. However, even if no sediment data is available at all, the two free sediment parameters D and ψ_c can still be tuned to represent wave observations; presently an almost complete lack of observations of roughness lengths k_N in previous models has been overcome in a similar way. In fact, the use of a moveable-bed model has an advantage, as D and ψ_c can be determined independently, whereas the roughness length k_N of previous models has to be tuned within the context of the model considered. This advantage is reduced, however, for multimodal or bioturbated sands, for which the determination of representative sediment parameters is not straightforward. Finally, the potential occurrence of a preferred swell height has the interesting implication that sediment data might be inferred from wave observations.

The discontinuous nature of initial ripple formation hampers direct implementation of a moveable-bed roughness model because (i) decay length scales associated with initial ripple formation [O(10 km), section 4b] are typically smaller than the grid size of a numerical model (typically 25–100 km), and because (ii) sediment conditions can show significant subgrid variations (e.g., Huntley and Hazen 1988; Amos et al. 1988; and Lyne et al. 1990), so that local sediment conditions in combination with a discontinuous roughness model might not result in a representative bottom friction source term for grid scales (e.g., Tolman 1991). Both points call for a subgrid approach to moveable-bed bottom friction. A subgrid approach has the additional advantage that it removes the discontinuity of the model. This simplifies numerical implementation and, furthermore, appears more realistic as the critical Shields number is not uniquely defined for irregular waves [Amos et al. (1988) in fact observed a transition zone of undeveloped ripples in conditions of initial ripple formation]. A subgrid version of the present model will be presented elsewhere.

7. Conclusions

Using the moveable-bed bottom friction model defined in sections 2 and 3, it is shown that typical swell cases can result in both smooth beds, on which no wave-induced sediment transport occurs, or in extremely rough beds, related to initial ripple formation. Typical depth-limited wind seas generally result in washed-out ripples and possibly in moderate sheet flow. The large change of bottom roughness for swell in conditions of initial ripple formation implies the possible occurrence of a preferred wave height, in particular for the bathymetric scales typical for shelf seas away from the coast. In such conditions, the bottom roughness is no longer locally defined, but depends on the spatial energy balance and hence on the two-dimensional bathymetry. This makes the availability of good sediment data important for the interpretation of swell decay rates. For wind seas, specific effects of moveable beds are not expected to dominate bottom friction or observations of depth-limited wave height.

It is shown that several nonlinear effects in the present model largely cancel for many practical conditions. This explains the apparent success of the empirical, quasi-linear JONSWAP model. In conditions where this model is expected to perform well, changes in friction factors appear to be dominated by hydrodynamic effects, which makes models using a single, predefined roughness potentially successful. None of these models, however, is expected to reproduce the above preferred wave height. Finally, a subgrid approach is required, if a moveable-bed model is to be implemented in a numerical wind wave model.

Acknowledgments. The author acknowledges with pleasure the help of Dean G. Duffy and Leo H. Holthuijsen in discussing early drafts of this paper. The constructive remarks of the referees contributed significantly to the paper. This study started while the author held a National Research Council–NASA Research Associateship and was finished while he held a UCAR visiting scientist position at NOAA/NMC.

APPENDIX

A One-Dimensional Steady Swell Decay Model

For a steady, one-dimensional swell field subject to shoaling and bottom friction only, the balance equation for the total energy E can be written as

$$\frac{\partial c_g E}{\partial x} = S_t = -\frac{1}{4g} f_w u_r^3, \qquad \text{(A1)}$$

where x is a coordinate along the beach slope and S_t is the source term integrated over the spectrum [from Eqs. (3) and (6)]. Equation (A1) is solved numerically using a fractional step method. A first estimate ($E_{i,p}$) of the energy E_i at grid point i is obtained by propagating the energy from the previous grid point. This first guess is corrected for the bottom friction given by Eqs. (3)–(14) (calculated from $E_{i,p}$)

$$E_i = E_{i,p} - \Delta E_{\text{bot}}, \quad E_{i,p} = \frac{c_{g,i-1}}{c_{g,i}} E_{i-1},$$

$$\Delta E_{\text{bot}} = \frac{\Delta t}{4g} f_w u_r^3, \quad \Delta t = \frac{\Delta x_i}{c_{g,i}}, \qquad \text{(A2)}$$

where Δt is the time step corresponding to the grid increment Δx [typically O(10 m)] and where c_g follows from the invariant period and the local depth. In case of ripple formation ($\psi/\psi_c \geq 1.2$), the application of ΔE_{bot} cannot result in $\psi/\psi_c < 1.2$. The corresponding

maximum energy loss due to bottom friction $\Delta E_{\text{bot,max}}$ is estimated from

$$\psi/\psi_c - \frac{\partial(\psi/\psi_c)}{\partial E}\,\Delta E_{\text{bot,max}} = 1.2 \qquad \text{(A3)}$$

as

$$\Delta E_{\text{bot,max}} = 2E\left(\frac{\psi/\psi_c - 1.2}{\psi/\psi_c}\right) \times \left(2 - \frac{D/a_r}{f'_w}\frac{\partial f'_w}{\partial(D/a_r)}\right)^{-1}. \qquad \text{(A4)}$$

If this limitation becomes effective, the representative friction factor becomes

$$f_w = \frac{4g\Delta E_{\max}}{u_{r,i}^3 \Delta t} \qquad \text{(A5)}$$

and the corresponding roughness k_N is given by Eq. (4).

REFERENCES

Amos, C. L., A. J. Bowen, D. A. Huntley, and C. F. M. Lewis, 1988: Ripple generation under combined influence of waves and currents on the Canadian continental shelf. *Contin. Shelf Res.*, **8**, 1129–1153.

Bouws, E., and G. J. Komen, 1983: On the balance between growth and dissipation in an extreme depth-limited wind-sea in the southern North Sea. *J. Phys. Oceanogr.*, **13**, 1653–1658.

——, H. Günter, W. Rosenthal, and C. L. Vincent, 1985: Similarity of the wind wave spectrum in finite depth water. 1: Spectral form. *J. Geophys. Res.*, **90**, 975–986.

Cacchione, D. A., and D. E. Drake, 1982: Measurements of storm generated bottom stresses on the continental shelf. *J. Geophys. Res.*, **87**, 1952–1961.

——, W. D. Grant, D. E. Drake, and S. M. Glenn, 1987: Storm-dominated bottom boundary-layer dynamics on the northern California continental shelf: Measurements and predictions. *J. Geophys. Res.*, **92**, 1817–1827.

Christoffersen, J. B., and I. G. Jonsson, 1985: Bed friction and dissipation in a combined current and wave motion. *Ocean Eng.*, **12**, 387–423.

Collins, J. I., 1972: Prediction of shallow water spectra. *J. Geophys. Res.*, 77(15), 2693–2707.

Dingler, J. R., and D. L. Inman, 1976: Wave-formed ripples in nearshore sands. *Proc. 15th Int. Conf. on Coastal Engineering*, Honolulu, ASCE, 2109–2126.

Drake, D. E., and D. A. Cacchione, 1986: Field observations of bed shear stress and sediment resuspension on shelves. *Contin. Shelf Res.*, **6**, 415–429.

——, and ——, 1989: Estimates of the suspended sediment concentration (C_a) and resuspension coefficient (γ_0) from near-bottom observations on the California shelf. *Contin. Shelf Res.*, **9**, 51–64.

——, ——, and W. D. Grant, 1992: Shear stress and bed roughness for combined wave and current flows over a rippled bed. *J. Geophys. Res.*, **97**, 2319–2326.

Glenn, S. M., and W. D. Grant, 1987: A suspended sediment stratification correction for combined wave and current flows. *J. Geophys. Res.*, **92**, 8244–8264.

Graber, H. C., and O. S. Madsen, 1988: A finite-depth wind-wave model. Part I: Model description. *J. Geophys. Res.*, **87**, 469–481.

Grant, W. D., and O. S. Madsen, 1979: Combined wave and current interaction with a rough bottom. *J. Geophys. Res.*, **84**, 1797–1808.

——, and ——, 1982: Movable bed roughness in unsteady oscillatory flow. *J. Geophys. Res.*, **87**, 469–481.

——, and ——, 1986: The continental-shelf bottom boundary layer. *Annu. Rev. Fluid Mech.*, **18**, 265–305.

——, A. J. Williams III, and S. M. Glenn, 1984: Bottom stress estimates and their prediction on the northern Californian continental shelf during CODE-1: The importance of wave-current interactions. *J. Phys. Oceanogr.*, **14**, 506–527.

Gross, T. F., A. E. Isley, and C. R. Sherwood, 1992: Estimation of stress and bed roughness during storms on the northern California shelf. *Contin. Shelf Res.*, **12**, 389–413.

——, and J. I. Collins, 1968: Spectral dissipation of finite-depth gravity waves due to turbulent bottom friction. *J. Mar. Res.*, **26**(1), 1–12.

Hasselmann, K., T. P. Barnett, E. Bouws, H. Carlson, D. E. Cartwright, K. Enke, J. A. Ewing, H. Gienapp, D. E. Hasselmann, P. Kruseman, A. Meerburg, P. Müller, D. J. Olbers, K. Richter, W. Sell, and H. Walden, 1973: Measurements of wind-wave growth and swell decay during the Joint North Sea Wave Project (JONSWAP). *Ergän Dtsch. Hydrogr. Z.*, Series A (8), Nr. 12, 95 pp.

Huang, N. E., S. R. Long, C.-C. Tung, Y. Yuan, and L. Bliven, 1983: A unified two-parameter wave spectral model for a general sea state. *J. Fluid Mech.*, **112**, 203–224.

Huntley, D. A., and D. G. Hazen, 1988: Seabed stresses in combined wave and steady flow conditions on the Nova Scotia continental shelf: Field measurements and predictions. *J. Phys. Oceanogr.*, **18**, 347–362.

Jonsson, I. G., 1963: Wave boundary layers. *Proc. 10th Congress, International Association for Hydraulic Research*, London, **I**, 85–92.

——, 1966: Wave boundary layers and friction factors. *Proc. 10th Int. Conf. on Coastal Engineering*, Tokyo, ASCE, 127–148.

——, 1980: A new approach to oscillatory rough turbulent boundary layers. *Ocean Eng.*, **7**, 109–152.

——, and N. A. Carlsen, 1976: Experimental and theoretical investigations in an oscillatory turbulent boundary layer. *J. Hydraul. Res.*, **14**, 45–60.

Kajiura, K., 1968: A model of the bottom boundary layer in water waves. *Bull. Earthquake Res. Inst.*, **46**, 75–123.

Lyne, V. D., B. Butman, and W. D. Grant, 1990: Sediment movement along the U.S. east coast continental shelf. I: Estimates of bottom stress using the Grant-Madsen model and near-bottom wave and current measurements. *Contin. Shelf Res.*, **10**, 397–428.

Madsen, O. S., and W. D. Grant, 1976: Quantitative description of sediment transport by waves. *Proc. 15th Int. Conf. on Coastal Engineering*, Honolulu, ASCE, 1093–1112.

——, and M. M. Rosengaus, 1988: Spectral wave attenuation by bottom friction: Experiments. *Proc. 21st Int. Conf. on Coastal Engineering*, Málaga, ASCE, 849–857.

——, Y.-K. Poon, and H. C. Graber, 1988: Spectral wave attenuation by bottom friction: Theory. *Proc. 21st Int. Conf. on Coastal Engineering*, Málaga, ASCE, 492–504.

——, P. P. Mathiesen, and M. M. Rosengaus, 1990: Movable bed friction factors for spectral waves. *Proc. 22d Int. Conf. on Coastal Engineering*, Delft, ASCE, 420–429.

Nielsen, P., 1981: Dynamics and geometry of wave-generated ripples. *J. Geophys. Res.*, **86**, 6467–6472.

——, 1992: *Coastal Bottom Boundary Layers and Sediment Transport*. World Scientific, 324 pp.

Ribberink, J. S., and A. Al-Salem, 1990: Bedforms, sediment concentrations and sediment transport in simulated wave conditions. *Proc. 22d Int. Conf. Coastal Engineering*, Delft, ASCE, 2318–2331.

——, and ——, 1991: Sediment transport, sediment concentrations and bedforms in simulated asymmetric wave conditions. Delft Hydraulics, Report H840, Part IV.

Shemdin, O., K. Hasselmann, S. V. Hsiao, and K. Heterich, 1978: Nonlinear and linear bottom interaction effects in shallow water. *Turbulent Fluxes through the Sea Surface, Wave Dynamics and Prediction. NATO Conf. Ser. V*, Vol. 1, 347–365.

Simons, R. R., A. J. Grass, and M. Mansour-Therani, 1992: Experimental study of waves and currents crossing at right angles. *Proc. 23d Int. Conf. on Coastal Engineering,* Venice, ASCE, 604–617.

SWAMP Group, 1985: *Ocean Wave Modelling.* Plenum Press, 256 pp.

SWIM Group, 1985: A shallow water intercomparison of three numerical wave prediction models (SWIM). *Quart. J. Roy. Meteor. Soc.,* **111,** 1087–1112.

Tolman, H. L., 1989: The numerical model WAVEWATCH: A third generation model for the hindcasting of wind waves on tides in shelf seas. Communications on Hydraulic and Geotechnical Engineering. Delft University of Technology, ISSN 0169-6548, Rep. No. 89-2, 72 pp.

——, 1991: A third-generation model for wind waves on slowly varying, unsteady and inhomogeneous depths and currents. *J. Phys. Oceanogr.,* **21,** 782–797.

——, 1992: An evaluation of expressions for wave energy dissipation due to bottom friction in the presence of currents. *Coastal Eng.,* **16,** 165–179.

——, 1993: An evaluation of expressions for wave energy dissipation due to bottom friction in the presence of currents—Reply to the discussion by Z. J. You. *Coastal Eng.,* **19,** 329–333.

Weber, S. L., 1991a: Eddy-viscosity and drag-law models for random ocean wave dissipation. *J. Fluid Mech.,* **232,** 73–98.

——, 1991b: Bottom friction for wind sea and swell in extreme depth-limited situations. *J. Phys. Oceanogr.,* **21,** 149–172.

Wiberg, P. L., and D. M. Rubin, 1989: Bed roughness produced by saltating sediment. *J. Geophys. Res.,* **94,** 5011–5016.

Wilson, K. C., 1989: Friction on wave induced sheet flow. *Coastal Eng.,* **13,** 371–379.